Letter

Electrooptic Modulation in Thin Film Barium Titanate Plasmonic Interferometers

Matthew J. Dicken, Luke A. Sweatlock, Domenico Pacifici, Henri J. Lezec, Kaushik Bhattacharya, and Harry A. Atwater

Nano Lett., **2008**, 8 (11), 4048-4052• DOI: 10.1021/nl802981q • Publication Date (Web): 11 October 2008

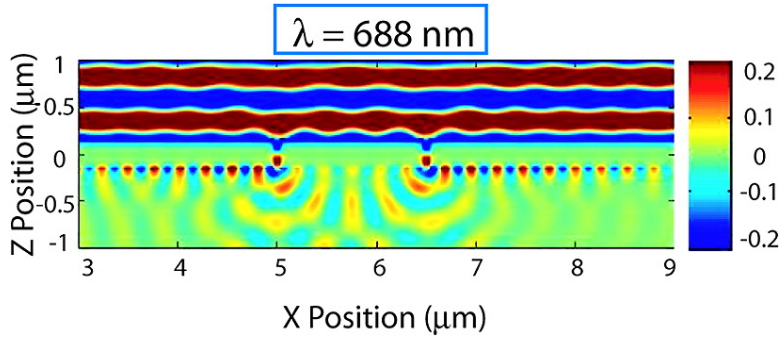

More About This Article

Additional resources and features associated with this article are available within the HTML version:

- Supporting Information
- Access to high resolution figures
- Links to articles and content related to this article
- Copyright permission to reproduce figures and/or text from this article

View the Full Text HTML

NANO LETTERS

2008
Vol. 8, No. 11
4048-4052

Electrooptic Modulation in Thin Film Barium Titanate Plasmonic Interferometers

Matthew J. Dicken,[†] Luke A. Sweatlock,[‡] Domenico Pacifici,[†] Henri J. Lezec,[§] Kaushik Bhattacharya,[†] and Harry A. Atwater*,[†]

Applied Physics, California Institute of Technology, Pasadena, California 91125, Northrop Grumman Space Technology, Redondo Beach, California 90278, and Center for Nanoscale Science and Technology, National Insitiute of Standards and Technology, Gaithersburg, Maryland 20899

Received October 1, 2008

ABSTRACT

We demonstrate control of the surface plasmon polariton wavevector in an active metal−dielectric plasmonic interferometer by utilizing electrooptic barium titanate as the dielectric layer. Arrays of subwavelength interferometers were fabricated from pairs of parallel slits milled in silver on barium titanate thin films. Plasmon-mediated transmission of incident light through the subwavelength slits is modulated by an external voltage applied across the barium titanate thin film. Transmitted light modulation is ascribed to two effects, electrically induced domain switching and electrooptic modulation of the barium titanate index.

The optical transmittance of arrays of subwavelength surface apertures in metal films, such as holes and slits, has generated enormous scientific interest, and surface plasmons have been found to play a governing role.[1−5] Surface apertures have been studied extensively as a means for coupling electromagnetic waves into and out of surface plasmon polariton (SPP) modes. Recently, passive plasmonic interferometers were constructed from pairs of slits as a means to enhance understanding of slit array transmittance.[6] Although at present these devices are only prototypical, ultracompact modulators derived from subwavelength slit arrays could have active areas less than 10 μm^2, compared to 1000 μm^2 for conventional electrooptic modulators.

SPPs are highly confined electromagnetic waves that propagate along a metal−dielectric interface by coupling to a polarization of the electron gas in the metal. Light can be coupled into and out of these modes by scattering from abrupt structural features such as grooves or slits.[7] The groundwork for passive plasmonic structures has been laid through intensive studies of SPP propagation in metal−dielectric structures.[8] It has been shown that these waves can interact with light transmitted through slits to create an interference pattern in the overall transmission intensity and this interference pattern can be affected by changes to the imaginary part of the SPP wavevector.[9] SPP modulation via the electrooptic effect has been studied previously in polymer films by coupling light into surface plasmon modes at a metal−polymer interface.[10] Here, we investigate dynamic modulation of the real part of the SPP wavevector by replacing the "dielectric" layer in the structure with an electrooptically active barium titanate thin solid film.

Barium titanate is a well-known perovskite ferroelectric material that exhibits a large electrooptic coefficient, on the order of $r = 100$ pm/V, and large birefringence due to its atomic structure, $\Delta n = 0.05$.[11,12] Thin films of barium titanate are deposited by numerous techniques, and their optical properties have been widely investigated and employed in electrooptic waveguides and modulators.[13−15] Barium titanate has a tetragonal crystal structure with an ordinary index, $n_o = 2.412$, corresponding to the shorter *a*-axis, which is larger than the extraordinary index, $n_e = 2.36$, along the *c*-axis. Ferroelectric domains form when the film is cooled below the Curie temperature (~120 °C) and their final orientation is affected by film stresses, as well as lattice and thermal expansion mismatch. Ferroelectric domains in barium titanate can be characterized by their orientation in-plane (*a*-axis) or out-of-plane (*c*-axis). Barium titanate thin films deposited on oxide thin film electrodes have been characterized by piezoresponse force microscopy and show both in-plane and out-of-plane domains.[16] These domains can be manipulated by applying an electric field across the material, and in-plane domains can be forced to switch out-of-plane under an

* Corresponding author.
[†] California Institute of Technology.
[‡] Northrop Grumman Space Technology.
[§] Center for Nanoscale Science and Technology.

10.1021/nl802981q CCC: $40.75
Published on Web 10/11/2008

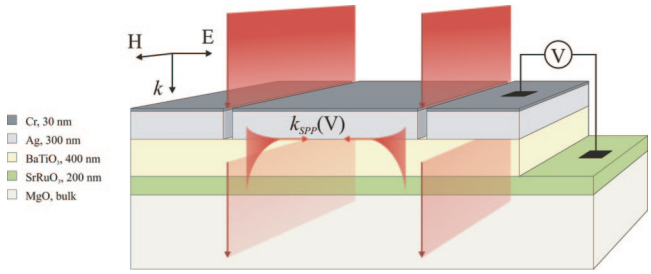

Figure 1. Schematic of a plasmonic modulator based on interference of SPPs launched from a set of parallel slits milled into a planar metal film. The counterpropagating SPPs travel with wavevector k_{SPP} along the Ag/$BaTiO_3$ interface. The interference of these SPPs with the transmitted fields can be affected by an applied voltage across the $BaTiO_3$ layer, by means of electrooptic modulation and electrically induced domain switching.

applied field greater than the coercive field. This domain switching event is accompanied by a large change in the index of the barium titanate thin film due to the birefringence in the material. Using barium titanate thin films, we modulate the real part of the index of refraction at the Ag/$BaTiO_3$ interface and thereby modulate the SPP wavevector.

Discussion. A schematic of the plasmonic interferometer based on double-slit transmission and electrooptic modulation of the SPP wavevector is shown in Figure 1. The optically active oxide thin film stack used for these SPP mediated double-slit interferometers was deposited without breaking vacuum in a pulsed laser deposition system (Neocera 180). Strontium ruthenate and barium titanate thin films were deposited on double-side polished magnesium oxide substrates (MTI Crystal). MgO substrates with dimensions 10 mm × 10 mm × 0.5 mm were attached to a molybdenum holder with silver paste for good thermal contact. Substrates were annealed at 900 °C for 1 h in vacuum ($P = 1 \times 10^{-7}$ Torr) prior to growth. The $SrRuO_3$ and $BaTiO_3$ films were deposited at 700 °C with background oxygen partial pressures $P_{O_2} = 150$ mTorr and $P_{O_2} = 10$ mTorr, respectively. The substrates were rotated 60 deg/s, and the target−substrate distance was kept at 9 cm during growth. A KrF excimer laser ($\lambda = 248$ nm) focused onto sintered targets of 99.9% pure $SrRuO_3$ and 99.99% pure $BaTiO_3$ was used to ablate the material at a pulse rate of 10 Hz with a pulse power of 300 mJ. After deposition, the films were cooled to room temperature at a rate of 5 deg/min at $P_{O_2} = 1$ Torr. The film thicknesses grown under these conditions were 400 nm barium titanate and 200 nm strontium ruthenate. The crystal structure of the samples was characterized by X-ray diffraction and reflection high-energy electron diffraction (RHEED). $\theta-2\theta$ X-ray scans were performed in a Panalytical X'PERT diffractometer using Cu Kα radiation ($\lambda = 1.5406$ Å). $\theta-2\theta$ X-ray scans show the epitaxial, single-crystalline phase (100/001), of the $BaTiO_3/SrRuO_3/MgO$ structure. RHEED was performed ex situ in a separate chamber equipped with a 25 keV electron gun. Silver (300 nm) and chromium (30 nm) films were vacuum deposited by evaporation onto the sample through a shadow mask to expose only a rectangular area on the sample. The structures consist of pairs of parallel slits etched into the metal layer by FIB milling (FEI Nova 600 dual beam focused ion beam system, Ga^+ ions, 30 keV).

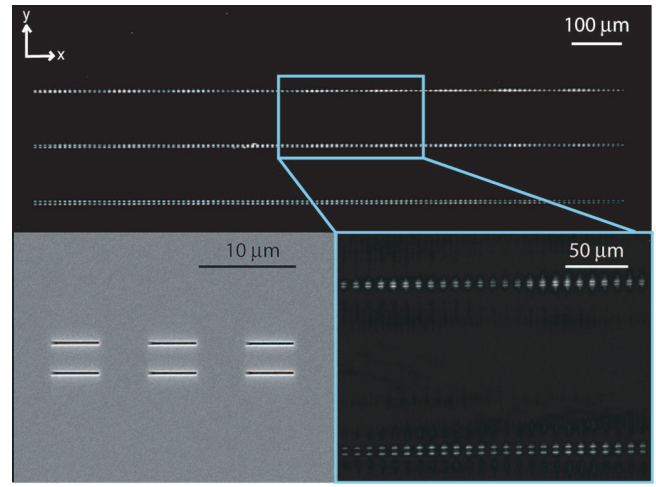

Figure 2. Double-slit SPP interferometer array. CCD image, collected with a 10× objective, of an array of double-slit devices patterned in Cr/Ag on $BaTiO_3$ illuminated by TM-polarized (H-field parallel to the long axis of the slit) 688 nm laser light. The slit pitch starts at 0.50 μm and increases by 20 nm for each device along a row. The observed intensity oscillation as a function of slit pitch is due to SPP interference with light transmitted through each slit. Insets: Scanning electron micrograph of slit pairs milled by focused ion beam in a chromium on silver layer. 50× image of devices with slit pitches varying from 1.50 to 1.98 μm showing one full period of transmitted intensity oscillation.

The slits are 5 μm long by 100 nm wide with slit pitch starting at 500 nm and increasing by 20 nm for each device along a row. Each device is laterally separated by 5 μm (Figure 2). Electrical contacts are made to the strontium ruthenate film by mechanically etching the barium titanate film and contacting the strontium ruthenate using conventional silver paste. The final device is mounted onto a glass slide, and copper tape is used to contact the top chromium/silver layer and bottom strontium ruthenate layer. A total of 240 plasmonic interferometers were investigated using these methods.

The device array is illuminated by a TM-polarized (H field parallel to the long axis of the slit) light source causing a fraction of the energy to be coupled into SPP modes at the Ag/$BaTiO_3$ interface and the remaining to be transmitted or reflected. The SPP mode extends evanescently into both the metal and ferroelectric films, and the SPP wavevector, k_{SPP}, is determined by the optical properties of both layers. The two counterpropagating surface waves are scattered out from the interface into radiative modes at the opposite slit. The SPPs interfere with the transmitted light at each slit corresponding to their phase accumulation during propagation along the interface. Interference with the transmitted light can be modulated by changing the SPP phase via slit pitch or SPP wavevector. We designed experiments, complemented by full field electromagnetic simulations, based on planar arrays of these devices (Figure 2) to investigate optical modulation in SPP-mediated double-slit interferometers.

A simple analytical treatment of the total transmitted intensity resulting from interference between the incident field and the SPP field can be used to show that small changes in the index of refraction of the dielectric layer can

lead to significant changes in the transmitted intensity profile. For this work, the double-slit device is governed by plasmon interference at the bottom interface of the Ag, due to the highly absorbing chromium layer at the top surface. Considering the transmission at each slit to be the sum of a transmitted field and a SPP field that has acquired some phase, $\phi = k_{SPP}x + \phi_o$, the resulting normalized transmitted intensity can be expressed as[17]

$$\frac{I_T}{I_o} = 1 + (\beta_o\beta_o')^2 e^{-\alpha x} + 2\beta\beta_o' e^{-(\alpha/2)x} \cos[k_{SPP}x + \phi_o] \quad (1)$$

where β_o and β_o' are scattering efficiencies for SPP coupling at each slit, α is the absorption coefficient, k_{SPP} is the SPP wavevector, and ϕ_o is the phase imparted by scattering from the slit. Data from experiments and full field electromagnetic simulations have been fit by this model to extract the relative index change of the active barium titanate layer from

$$n_{SPP} = \sqrt{\varepsilon_{Ag}\varepsilon_{Eff}/(\varepsilon_{Ag} + \varepsilon_{Eff})}$$

where ε_{Eff} is an effective dielectric constant describing the properties of all nonmetallic layers.[18]

To explore the physics of this double-slit device, simulations were performed using full field finite-difference time-domain software (FDTD).[19] A multioscillator Lorentz−Drude model is used for the chromium and silver layers with parameters given by Rakic et al.[20] The barium titanate and strontium ruthenate complex refractive index data were derived from variable-angle spectroscopic ellipsometry measurements.[21] Figure 3a shows the magnetic field profile (H_y) for one device with a slit pitch of 1.50 μm and an index of refraction, n_{BTO}, of 2.20 for the barium titanate layer. The input plane wave ($\lambda = 688$ nm) from $Z = 1$ μm is transmitted through the 100 nm wide slits, and a fraction is scattered into surface plasmon polariton modes propagating along the Ag/$BaTiO_3$ interface to the left and right of each slit. Counterpropagating SPPs along the interferometer arm formed between the slits interfere constructively or destructively depending on slit pitch and SPP wavevector. Figure 3b shows the absolute magnetic field (H_y^2) from the same simulation. The resonant mode formed by the two counterpropagating SPPs inside the cavity can be identified in this figure. SPPs propagating away from each slit appear in the form of a continuously decaying intensity profile along the Ag/$BaTiO_3$ interface. Figure 3b also shows fields being coupled into a waveguide mode formed by the 400 nm barium titanate film.

At each slit, a fraction of the incoming energy scatters out of the SPP mode and interferes with the transmitted light to create an overall modulation in the transmitted power. The optical power flow through the device can be analyzed for these simulations by plotting the Poynting vector (S_z) (Figure 3c). A monitor line placed along the bottom of the simulation ($Z = -1$ μm) can be used to monitor the net "transmission", that is, the power flow away from the slit pair in the $-z$ direction. Plotting the integrated power flow out of the device for each slit pitch yields an interference pattern as predicted from theory (Figure 4a). Simulations were done for these devices using input barium titanate indices of refraction of 2.20 and 2.21 to approximate the

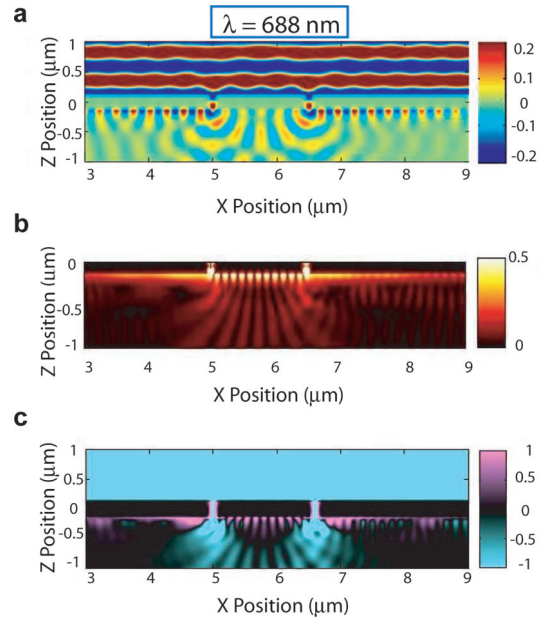

Figure 3. FDTD device simulations. Full-field finite difference time domain simulations of a double-slit SPP interferometer device with a slit pitch of 1.50 μm illuminated by $\lambda = 688$ nm plane-wave light. (a) Magnetic field (H_y) distribution for the device structure showing the destructive interference of the counterpropagating SPPs between the slits. (b) Absolute magnetic field (H_y^2) showing the standing wave mode formed by the counterpropagating SPPs as well as the slowly decaying SPPs propagating away from each slit. (c) Power flow (S_z) simulation used to quantify the relative power leaving the modeled devices at position $Z = -1$ along the X position.

index change under applied bias. The range of indices simulated is indicative of a change in index due to some degree of a-domain to c-domain switching under bias. These FDTD data were fit using eq 1 to extract n_{SPP} and n_{Eff} following from $\varepsilon_{Eff} = n_{Eff}^2$. We find that comparing simulations with $n_{BTO} = 2.20$ and 2.21, the model fit yields $n_{SPP} = 2.626$ and 2.646 from which $n_{Eff} = 2.24$ and 2.25, respectively, corresponding to a change $\Delta n_{Eff} = 0.01$ (Figure 4a). The difference in n_{Eff} from the input n_{BTO} is due to SPP interaction with the entire material stack beneath the barium titanate, which is naturally addressed in the FDTD simulation, but not the analytical model. This does not affect the overall change in index, both the input and simulated index change are $\Delta n = 0.01$. It is important to note that the intensity of the modulation is indicative of the change in n_{SPP} for a given slit pitch and material index and can be used to put a lower limit on the index change for a given device. The percent change in integrated power flow for each device, as n_{BTO} is changed from 2.20 to 2.21, is plotted in Figure 4b. We can infer that the smallest change in n_{Eff} to yield 15% modulation for a device with pitch 2.26 μm with the optical material properties simulated here is $\Delta n_{Eff} = 0.01$.

We fabricated an array of double-slit interferometer structures in silver on barium titanate (Figure 2). The double-slit device array was illuminated from the topside, normal to the sample, with a TM-polarized ($\lambda = 688$ nm) diode laser source. The diode laser was aligned to the optical axis of a Zeiss Axiovert 135 inverted microscope using a quartz cube

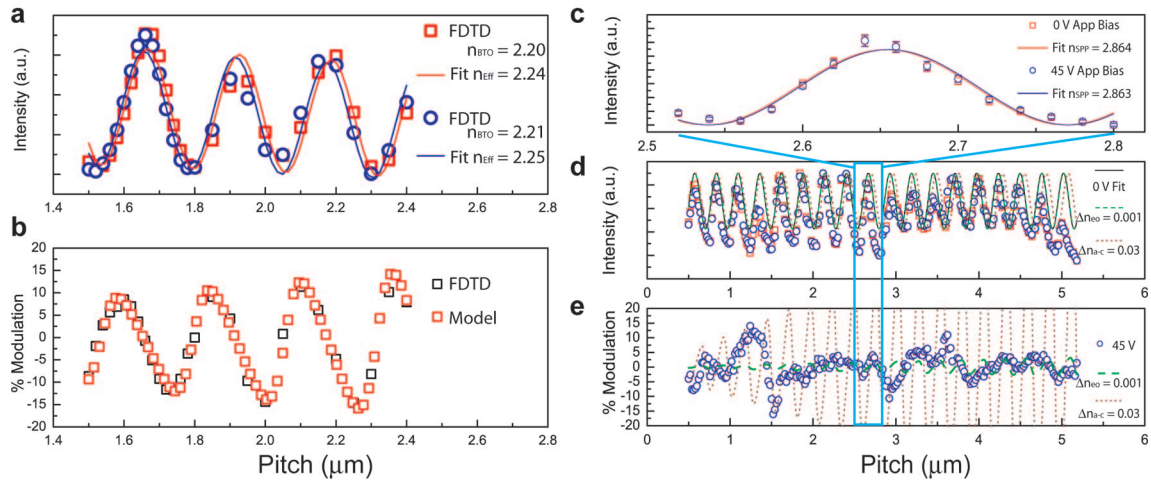

Figure 4. FDTD and analytical model validation. Integrated power flow from FDTD simulations of devices from 1.50 to 2.40 μm and experimental results for devices from 0.50 to 5.25 μm fit using eq 1. (a) FDTD data for barium titanate indices of $n_{BTO} = 2.20$ and 2.21. The model fit for these results yields SPP indices of $n_{SPP} = 2.626$ and 2.646 and the extracted $n_{Eff} = 2.24$ and 2.25. (b) Signal modulation from both FDTD data and model fit agree well. (c) Analytical model fits for experimental device response with pitches 2.52−2.80 μm show an electrooptical change in the index of $\Delta n_{SPP} = 0.001$. (d) Experimental data and fits for devices at 0 and 45 V. The dashed lines are theoretical interference patterns corresponding to $\Delta n = 0.001$ and 0.03 for electrooptic and domain reorientation effects, respectively. (e) Experimental data for devices under 45 V applied bias show modulation up to 15%, compared to 0 V. The dashed lines are the theoretical modulation for changes in index of $\Delta n = 0.001$ and 0.03. Devices in the range 1.75−2.75 μm show modulation on the order of the electrooptic effect while devices from 1.00 to 1.50 μm show much larger modulation due to domain reorientation.

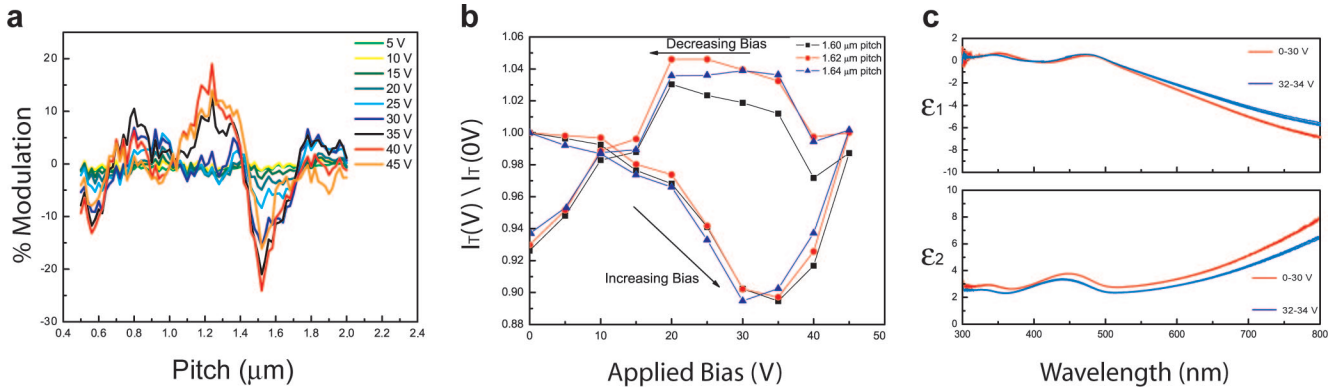

Figure 5. Experimental observation of SPP modulation. Data collected by inverted microscope and spectroscopic ellipsometer show evidence of optical index change inducing modulation in propagating SPPs. (a) Experimentally measured signal modulation for devices in the range of 0.50−2.0 μm slit pitch, under polarized $\lambda = 688$ nm light. The intensity modulation shows areas where index change is on the order of electrooptic effect and a-domain to c-domain switching induced. The large signal increase between 30 and 35 V is attributed to a−c domain switching. (b) Devices in the pitch range where the largest modulation occurs show expected hysteretic behavior due to domain relaxation. (c) Spectroscopic ellipsometry confirms large index change, on the order of $\Delta n = 0.03$, between 30 and 32 V applied bias.

beamsplitter. The laser spot was expanded to uniformly cover the 2 mm by 2 mm device array and approximate a plane wave source from the Gaussian beam. A microscope objective (10×, N.A. 0.25) was used to collect transmitted light into a liquid nitrogen cooled silicon CCD camera. A clear modulation in the transmitted intensity can be seen in the first and second rows, where the device pitch varies from 0.50 to 5.28 μm. At 50× (NA = 0.45) magnification (Figure 2, inset) a clear distinction between each slit can be seen, as well as one full period of intensity oscillations due to the interference of the out-coupled SPPs with the transmitted light.

The intensity profile along each row of devices under both zero and applied bias was monitored to understand the dynamic switching properties of the interferometer. The overall transmitted intensity from each device was integrated over the device area and compared along each row. Figure 4d shows transmission data from the first two rows of devices (pitch 0.50−5.28 μm) with an expanded view of devices spanning the pitch range 2.52−2.80 μm. Devices in pitch range 2.52−2.80 μm were fit using the analytical model (eq 1) and show an electrooptic change in the SPP index of $\Delta n_{SPP} = 0.001$ at 45 V applied bias (Figure 4c). Modulation of the transmitted intensity profile for all devices in the range shows up to 15% change in the signal compared to 0 V. A change in index of this magnitude suggests some degree of a-domain to c-domain switching in the active barium titanate layer. The intensity modulation data also suggest that each device did not undergo the same change in n_{SPP}. To investigate this further, we plotted the theoretical change in both the

interference pattern and the percent modulation approximating electrooptic switching ($\Delta n_{eo} = 0.001$) and domain switching ($\Delta n_{a-c} = 0.03$) effects (Figure 4e). We also observed that in some regions the device transmittance departed from the prediction of the analytic model due to local changes in n_{Eff} arising from changes in either the Ag/$BaTiO_3$ index or local film inhomogeneities. Intensity data were compiled in 5 V increments from 0 to 45 V and the percent change in intensity compared to 0 V is plotted in Figure 5a. We see a reasonable comparison of the modulation data for devices with pitches in the range 0.50−1.00 μm with theoretical modulation due to electrical modulation of the SPP wavevector, via domain switching effects on the order of $\Delta n_{Eff} = 0.03$. For slit pitches less than 1.00 μm, the maxima and minima of the intensity modulation correspond well with the inflection points of the 0 V interference pattern. This implies that the change in index from device to device was similar in this range. Devices between 1.00 and 1.80 μm slit pitch show the largest change in intensity modulation. By comparing the data in this range to the percentage modulation of the analytical model, we can put a lower limit of $\Delta n_{Eff} = 0.03$ on the index change in these devices. This larger effect is attributed to domain switching or piezoelectric activity in the barium titanate film, such that devices showing very large intensity modulation are undergoing 90° domain switching from *c*-axis in-plane to *c*-axis out-of-plane.[16] This effect would yield a change in the index of refraction on the order of the birefringence of the material, $\Delta n = 0.05$. The fraction of domains that switch between the slits of each device will dictate the change in effective index for the device.

To investigate this further, the bias across the devices was cycled from 0 to 45 to 0 V. A plot of the response of three devices (1.60, 1.62, 1.64 μm slit pitch) to the voltage cycle is shown in Figure 5b. The intensities of these devices were normalized to their values at 0 V. The device response shows hysteresis demonstrative of ferroelectric domain switching. As the bias is increased, devices in this range show a decrease in output intensity as the index changed up to 35 V, and the following increase in intensity suggests that the index change was sufficient to move the response through a minimum in the interference pattern. As the bias is decreased, the domains that have switched from *c*-axis in-plane to *c*-axis out-of-plane relax slowly to their original state. At 15 V, decreasing bias, the index begins to follow the same path through the intensity minimum.

Finally, we performed an independent confirmation of the large refractive index change due to domain switching. This effect was investigated using spectroscopic ellipsometry in a separate planar sample with a 20 nm, optically transparent, silver film evaporated on the same $BaTiO_3/SrRuO_3/MgO$ film stack. Shown here (Figure 5c) are the ε_1 and ε_2 data, as measured by variable angle spectroscopic ellipsometry, under applied voltage from 0 to 35 V. The change in ε_1 and ε_2 at 30 V corresponds to $\Delta n = 0.03$ at 688 nm, which is on the order of the change due to domain switching seen in the plasmonic interferometers.

The phenomenon of SPP-mediated interference using a pair of subwavelength slits in silver on barium titanate thin films has been investigated by a simple analytical model, full field finite difference simulations, and experiment. Electrical modulation of the SPP wavevector was achieved by utilizing the electrooptic effect as well as 90° domain switching in barium titanate. The degree of optical switching obtained in these devices is potentially useful for designing new plasmonic and metamaterial structures in which active oxide replaces a static dielectric material. As photonic networks become more prevalent in chip-based microelectronic systems, the need for active nanoscale devices is increasingly apparent. Active plasmonic devices, based on electrooptic modulation, are well suited to fill this nanophotonic niche.

Acknowledgment. We acknowledge financial support from the National Science Foundation, under Grant DMR 0606472, and the Army Research Office; portions of this work were performed in facilities sponsored by the Center for Science and Engineering of Materials, an NSF MRSEC. We also gratefully acknowledge helpful discussions with Jennifer Dionne, Rene DeWaele, and Stanley Burgos.

References

(1) Thio, T.; Pellerin, K. M.; Linke, R. A.; Lezec, H. J.; Ebbesen, T. W. *Opt. Lett.* **2001**, *26* (24), 1972–1974.
(2) Ebbesen, T. W.; Lezec, H. J.; Ghaemi, H. F.; Thio, T.; Wolff, H. J. *Nature* **1998**, *391*, 667–669.
(3) Garcia-Vidal, F. J.; Lezec, H. J.; Ebbesen, T. W.; Martin-Moreno, L. *Phys. Rev. Lett.* **2003**, *90*, 213901.
(4) Lezec, H. J.; Thio, T. *Opt. Express* **2004**, *12*, 3629–3651.
(5) Gay, G.; Alloschery, O.; Lesegno, B. V. e.; O'Dwyer, C.; Weiner, J.; Lezec, H. J. *Nat. Phys.* **2006**, *2*, 262–267.
(6) Schouten, H. F.; Kuzmin, N.; Dubois, G.; Visser, T. D.; Gbur, G.; Alkemade, P. F. A.; Blok, H.; tHooft, G. W.; Lenstra, D.; Eliel, E. R. *Phys. Rev. Lett.* **2005**, *94*, 053901.
(7) Lalanne, P.; Hugonin, J. P.; Roier, J. C. *Phys. Rev. Lett.* **2005**, *95*, 263902.
(8) Dionne, J. A.; Lezec, H. J.; Atwater, H. A. *Nano Lett.* **2006**, *6*, 1928–1932.
(9) Pacifici, D.; Lezec, H. J.; Atwater, H. A. *Nat. Photonics* **2007**, *1*, 402–406.
(10) Chyou, J. J.; Chu, C. S.; Shih, Z. H.; Lin, C. Y. *Opt. Eng.* **2005**, *44* (3), 034001.
(11) Zgonik, M.; Bernasconi, P.; Duelli, M.; Schlesser, R.; Gunter, P. *Phys. Rev. B* **1994**, *50*, 5941–5949.
(12) Beckers, L.; Schubert, J.; Zander, W.; Ziesmann, J.; Eckau, A.; Leinenbach, P.; Buchal, C. *J. Appl. Phys.* **1998**, *83*, 3305–3310.
(13) Petraru, A.; Schubert, J.; Schmid, M.; Buchal, C. *Appl. Phys. Lett.* **2002**, *81*, 1375–1377.
(14) Tang, P.; Towner, D. J.; Hamano, T.; Meier, A. L.; Wessels, B. W. *Opt. Express* **2004**, *12*, 5962–5967.
(15) Tang, P.; Towner, D. J.; Meier, A. L.; Wessels, B. W. *Appl. Phys. Lett.* **2004**, *85*, 4615–4617.
(16) Kim, I. D.; Avrahami, Y.; Tuller, H. L.; Park, Y. B.; Dicken, M. J.; Atwater, H. A. *Appl. Phys. Lett.* **2005**, *86*, 192907.
(17) Pacifici, D.; Lezec, H. J.; Weiner, J.; Atwater, H. A. *Phys. Rev. B* **2008**, *77*, 115411.
(18) Raether, H. *Surface plasmons on smooth and rough surfaces and on gratings*; Springer: Berlin, 1988; Vol. 111, pp 1−133.
(19) *Finite-Difference Time-Domain Simulation Design Software (OptiFDTD)*; Optiwave Systems Inc., 2005.
(20) Rakic, A. D.; Djurisic, A. B.; Elazar, J. M.; Majewski, M. L. *Appl. Opt.* **1998**, *37* (22), 5271–5283.
(21) Dicken, M. J.; Diest, K.; Park, Y. B.; Atwater, H. A. *J. Cryst. Growth* **2007**, *300*, 330–335.

NL802981Q